Leppänen, J.; Ross, G.; Vuorinen, V.; Ingman, J.; Jormanainen, J.; Paulasto-Kröckel, M.

A humidity-induced novel failure mechanism in power semiconductor diodes

Published in:
Microelectronics Reliability

DOI:
10.1016/j.microrel.2021.114207

Published: 01/08/2021

Document Version
Publisher's PDF, also known as Version of record

Microelectronics Reliability 123 (2021) 114207

Contents lists available at ScienceDirect

Microelectronics Reliability

journal homepage: www.elsevier.com/locate/microrel

A humidity-induced novel failure mechanism in power semiconductor diodes

J. Leppänen [a,*], G. Ross [b], V. Vuorinen [b], J. Ingman [a], J. Jormanainen [a], M. Paulasto-Kröckel [b]

[a] ABB Drives, Finland
[b] Aalto University, Finland

ARTICLE INFO

Keywords:
H3TRB
THB
IGBT
EoL
PoF
LiT
FIB
STEM

ABSTRACT

Power electronics reliability in a high humidity environment has recently been considered an important aspect of power converters. In this article boost stage power semiconductor modules from two vendors with varying device technologies were exposed to high humidity, high temperature and high voltage reverse bias direct current (H3TRB-HVDC) test conditions. The exposed modules were monitored with in situ leakage current measurement during the test. The in situ monitoring revealed that all samples from one vendor using a glass passivation technique failed while the samples from the second vendor with a polyimide passivation survived. After the test, electrical breakdown and associated thermal hotspots were consistently observed using lock-in thermography on top of the glass passivation covering the high voltage edge termination structure. It was concluded with microstructural and material analysis that the treelike structures that were observed right beneath the surface of the glass passivation were associated with the failure mechanism. The analysis revealed that the formed structures were amorphous and could not be caused by the electrochemical migration of metallic species. The failures were caused by the localised partial dissolution of lead from the glass passivation. The failure mechanism seems to be associated with water treeing.

1. Introduction

During previous decades, the usage of power semiconductor modules based on devices – for example insulated gate bipolar junction transistors (IGBTs), power metal oxide semiconductor field effect transistors (MOSFETs) and power diodes – have expanded into a wider range of power conversion applications than before, leading to an increasing amount of relatively harsh environmental use cases. Power semiconductor devices tend to have high field failure rates, especially in environmentally demanding applications (e.g. wastewater management, offshore wind converters and photovoltaic solar inverter solutions). Therefore, humidity, temperature and corrosive environmental conditions must be considered in power electronics design. Many of the encountered failures are considered early failures, occurring within less than 5–10 years after commissioning. This short lifetime is insufficient for power electronics–based power conversion systems that are intended to be used for >20 years [1–4]. Power converter manufacturers utilising power semiconductor modules have recently acknowledged that the housing cannot be completely hermetically sealed with cost-effective means. To meet the expected lifetime, the power device's environmental robustness must be addressed. This is one of the many reasons why there is a trend towards developing system-level reliability in power electronics, which requires understanding physical wear-out mechanisms in realistic environmental conditions [1]. Therefore, reliability engineering based on Design for Reliability (DfR) is becoming a common development approach in power electronics [4] and the Physics of Failure (PoF) methodology is adopted in combination with DfR, requiring component-level end-of-life (EoL) tests [5,6].

Several failure mechanisms of power electronic systems have been identified, both on chip level [7] and package level [8], induced by temperature humidity bias (THB) tests demonstrating EoL (i.e. premature voltage blocking breakdown). On the chip level the high voltage edge termination structures seem to be the most vulnerable regions since electrochemical migration (ECM) has been observed on top of the passivation films (polyimide or glass) and beneath the passivation between the metallic guard rings (GR) [7]. These mechanisms are described as *dendritic growth* and *aluminum corrosion* respectively [9]. Furthermore, on the package level, failure mechanisms have been also reported to be induced by ECM on the high voltage insulation trenches of the direct copper bonded (DCB) substrate between the high voltage

* Corresponding author.
E-mail address: joonas.leppanen@fi.abb.com (J. Leppänen).

https://doi.org/10.1016/j.microrel.2021.114207
Received 9 February 2021; Received in revised form 29 April 2021; Accepted 13 June 2021
Available online 1 July 2021

copper tracings. DCB insulation failures seem to be induced by humidity-temperature-voltage bias conditions when H_2S corrosive gas is present [8]. Due to these findings, there is a growing concern regarding the humidity robustness of non-hermetic or unmolded power semiconductors devices. Generally, the suspected deterioration mechanisms occur under reverse bias voltage [10,11].

Most of the standards regarding THB tests are limited to low or zero voltage, for example, JEDEC JESD-A101 [12] and IEC 60749–5 [13] describe the THB test at a low test voltage ($U_r \leq 80$ V) level. For high voltage power semiconductor devices, a low test voltage cannot reach EoL in a reasonable test duration [7,14]. An improved THB test method is the high humidity, high temperature and reverse bias high voltage direct current (H3TRB-HVDC) test, which is merely revised from the original [12,13] standards by increasing the test voltage.

The applicability of the test method was evaluated in [10] for silicon carbide (SiC) MOSFETs and in [15,16] for silicon (Si) power semiconductor devices (e.g. IGBTs and diodes). This test can be used as an accelerated life test (ALT) to initiate EoL failure mechanisms in a reasonable test duration related to the THB in modern Si/SiC-based non-hermetic power semiconductor devices.

In this article two converter designs with similar package topologies will be compared. The semiconductor device chip-level designs may vary from vendor to vendor. In Section 2 the test concept and relevant EoL failure mechanisms are reviewed, Section 3 describes a single failure mechanism in detail and discusses the possible processes involved. Finally, Section 4 concludes this article, providing suggestions for further studies.

2. Materials & methods

2.1. The H3TRB-HVDC test concept

An H3TRB-HVDC test is used to evaluate robustness against humidity under high reverse bias voltage conditions. A reverse bias direct current (DC) voltage was used, equivalent to 80% of the maximum reverse bias voltage, $U_{r,\ max}$, specified in the datasheets of the device. This bias voltage was kept constant until failure, which is defined either as deteriorated breakdown voltage ($U_{BR} < U_{r,\ max}$) or increased leakage current, I_r. Quantitatively this is defined as doubling the initial leakage current, which is monitored in situ during the test. However, in some cases even a short circuit can be observed. Test specification was already discussed in [10] and a summary is collected in Table 1 as a test specification.

Based on earlier studies [7,10,11], there are two electrical deterioration modes expected during the test described in Fig. 1. The failure behavior is reported to be seen either as an increasing leakage current or as a premature voltage breakdown when compared with the reference curve tracer measurements done prior to the H3TRB test [9,17].

Leakage characteristics can be measured prior to and after the test with commercial curve tracers, such as Keysight B1506. However, the maximum allowed voltage defined in the device datasheet should not be exceeded in order to protect the device from electrical overstress damage; thus, sometimes the nominal voltage breakdown cannot be seen. Due to the applied reverse bias voltage, the electric field over the power

Table 1
A summary of the H3TRB-HVDC test specification [10].

Symbol	Parameter	Values
rH	Relative humidity	85%
T_{amb}	Ambient temperature	85 °C
U_r	Reverse bias voltage	0.8 × $U_{r,\ max}$
U_G	Gate voltage	0 V
t_d	Test duration	1200 h
I_r	Failure criteria	$I_r \geq 2 \times I_{r,\ ref}$
$N \geq N_{min}$	Sample size	Min. 6 pcs (modules) Min. 6 pcs (chips)

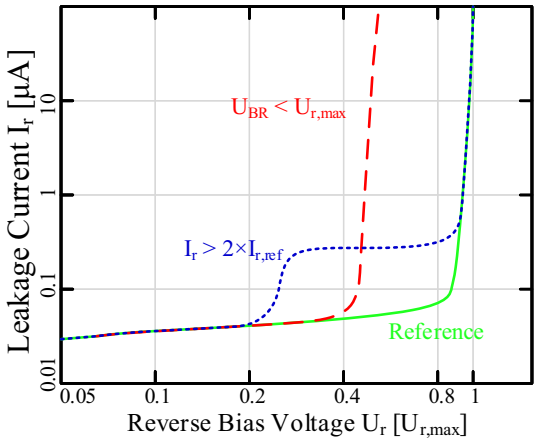

Fig. 1. The reverse bias leakage characteristic curve (the green solid line) shows the reference reverse voltage blocking characteristics of a nominal device, (the red dashed line) shows a decreased breakdown voltage and (the blue dotted line) shows a premature increase of the leakage current. (For interpretation of the references to colour in this figure legend, the reader is referred to the web version of this article.)

semiconductor device is arranged as pictured in Fig. 2 for a simple power semiconductor diode using field limiting ring (FLR) edge termination (ET) structures [18,19].

It is crucial to remember the direction of the electric field gradient in reverse bias conditions when considering possible failure mechanisms, for example electrochemical corrosion (EC) and associated migration directions, based on the actual ionic species in question. In Fig. 2 it is demonstrated that the top electrode (U_r-) is equivalent to the P-side (anode) and the bottom electrode (U_r+) is the N-side cathode in a diode configuration when reversely biased [18]. Similar devices are used either as an anti-parallel diode in buck/boost converter topologies and also in different rectifying bridge topologies [20,21].

In this experiment, boost converter modules consisting of a system of transistors (3–4 chips in parallel) and anti-parallel diodes (1–2 chips in parallel) from two vendors (A and B) were compared. From both vendors there were two different power ratings: 50 kW (low power) and 60 kW (high power) boost stage modules with a single voltage ($U_{r,\ max} = 1.2$ kV) rating. Seven modules from each vendor for each power rating were tested. Vendor A used glass passivation (based on lead oxide silica PbO-SiO_2) [22] while vendor B used polyimide (PI) passivation to protect the edge termination.

After the test, a few modules were selected for further failure analysis based on their deteriorated voltage blocking or leakage behavior as observed in a basic electric characterisation with a curve tracer. The silicone gel of the modules was removed by inserting the samples into a

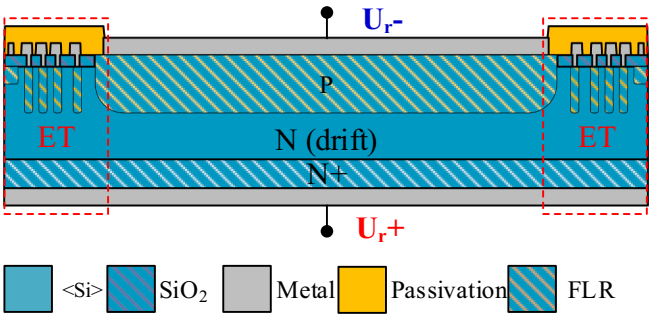

Fig. 2. A power semiconductor diode reverse biased with its ET structures based on FLRs (red dashed boxes). (For interpretation of the references to colour in this figure legend, the reader is referred to the web version of this article.)

sulfonic acid–based chemical (Chemetal ARDOX-2312) for 12–15 h at room temperature and then rinsed with de-ionised water, acetone and isopropyl alcohol and afterwards rinsed with nitrogen gas. Lock-in thermography (LiT) microscopy was used to localise the failure hot-spot using Optotherm Sentris LiT. Further analysis using scanning electron microscopy (SEM), energy dispersive X-ray (EDX) spectroscopy, focused ion beam (FIB) cross-sectioning and scanning transmission electron microscopy (STEM) was used where needed.

2.2. H3TRB-related failure mechanisms

Electrochemical corrosion (EC) is considered to be one of the most often occurring deterioration mechanisms of bare metal plates exposed to elevated temperatures and high relative humidity [23,24]. In principle, EC is defined as a metal losing some of its electrons to become an ion. This process eventually consumes the metal since the ionic metals typically dissolve into an aqueous solution (water or moisture) [23] or, rarely, into a solid that acts as an electrochemical cell [25]. The electrolytic cell formed by the water film between two electric potentials is the most important reaction required by the EC processes. This sort of a solution can be formed between two consecutive FLRs or GRs in the ET structure, as described in [17]. A schematic representation of the structure is depicted in Fig. 3 with a four-GR design, including a field plate (FP) structure. The purpose of the structure is to gradually terminate the electric field by shifting the depletion region boundary (DRB) further towards the edge, closer to the FP [19,26]. A recent article based on simulation results discussed electrical field increase in the ET region, both on top of the passivation film and beneath the passivation, when exposed to humidity [14].

The exact composition of the resulting electrolytic solution determines the properties of the solution. The process begins with the electrochemical overpotential (>1.67 V) of water [24,27], leading to the decomposition of water molecules into hydrogen and hydroxide ions [23,24]. The phenomenon is known as *electrolysis of water* (i.e. hydrolysis). In [7] this is suggested to occur when high voltage reverse bias conditions are applied and moisture is agglomerated on top of the edge termination passivation film or, eventually, beneath the passivation film protecting the edge termination, as shown in Fig. 3. At the electric anode the water molecules decompose into hydrogen ions and oxygen molecules [23,24,27]:

$$2H_2O \rightarrow O_2 + 4H^+ + 4e^-. \quad (1)$$

At the cathode a chemically reductive reaction builds up hydroxide ions and hydrogen gas [23,24,27]:

$$2H_2O + 2e^- \rightarrow H_2 + 2(OH)^- \quad (2a)$$

$$2H_2O + O_2 + 4e^- \rightarrow 4(OH)^-. \quad (2b)$$

At the anode, according to Eq. (1), it is suggested that the pH << 7, and respectively, at the cathode, according to Eqs. (2a) and (2b), the pH >> 7 (i.e. a large pH gradient exists between the anode and the cathode) [28,29]. These facts arise from the accumulation of OH^- ions at the cathode and H^+ ions at the anode side, as summarised in Fig. 4a.

The pH gradient can be associated with the ECM of metallic species, as described with Cu, Ag [7], Sn [28,29], and Pb [30]. Fig. 4b shows a basic example of the ECM process of positive metal ions from anode to cathode and the forming of a dendritic structure based on the dissolution of M^{n+} in a low pH solution [31]:

$$M \rightarrow M^{n+} + ne^-. \quad (3)$$

If, on the other hand, a protective oxide film is grown, the only possible starting locations for the process depicted in Eqa. (2a) and (2b) to occur are film pits or defects in the protective oxide film [32]. However, one must consider that there are several other chemical impurities that may act as reaction accelerators, like oxygen, since the incorporated ions may also drastically accelerate chemical corrosion reactions. These include, for example, Br^-, Cl^-, Na^+ and K^+, all of which affect the electrolytic solution facilitated by moisture, as discussed in [16,25,31,33,34]. Chemical impurities may cause a dramatic difference in the electrochemistry involved with the failure mechanisms, for example, the presence of hydrogen sulfide (H_2S) at a high concentration (50 ppm) was reported to produce copper sulfide dendrites on top of the IGBT package-level high voltage isolation [8]. Furthermore, for example, with aluminum, more complex electrochemical processes are involved, culminating in the creation of aluminum tetra hydroxide Al $(OH)_3 + OH^- \leftrightarrow [Al(OH)_4]^-$ [7,15,16]. Finally, it can be noted that the direction of the dendritic growth is determined by the direction of the electric field and associated migrating ion charge polarity.

3. Results & discussion

Based on the in situ monitoring during the H3TRB-HVDC test, all booster modules from vendor A failed between 900 and 1200 h due to a short circuit while their competing counterparts from vendor B with a passivation based on polyimide (PI) survived the test with only a single failure, as can be seen in Fig. 5. A single booster module from vendor A (high power) was removed from the statistics since it was mechanically damaged during the preparation of the test.

The failures were detected by in situ leakage current monitoring and the associated channel power supply was cut manually shortly afterwards. After the test was completed, an electrical characterisation was made for all samples with a curve tracer, as shown in Fig. 6a.

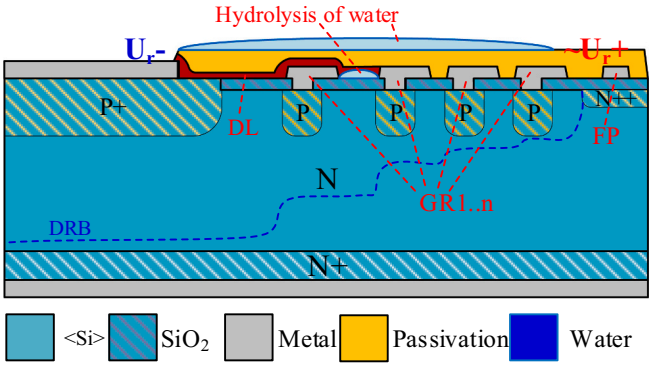

Fig. 3. Moisture can agglomerate onto the surface of the passivation or enter the area between two GRs or FPs due to the delamination (DL) of the passivation (shown in dark red), as described in [7,14,17]. (For interpretation of the references to colour in this figure legend, the reader is referred to the web version of this article.)

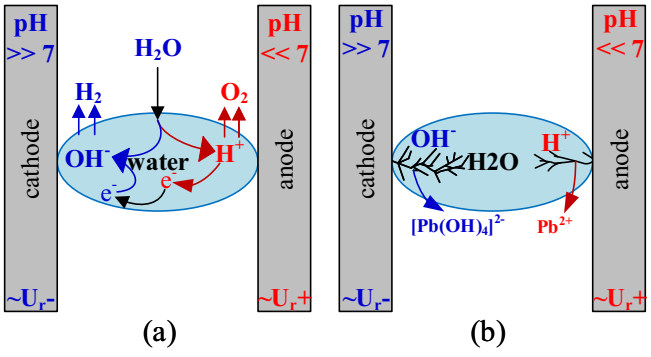

Fig. 4. Hydrolysis (a) leads into a large pH gradient [7,23] between cathode-anode electrodes forming an electrolytic cell, which can lead into (b) the ECM of some metallic species, e.g. Cu, Ag, Al, Pb, forming a dendrite between cathode and anode [7,30].

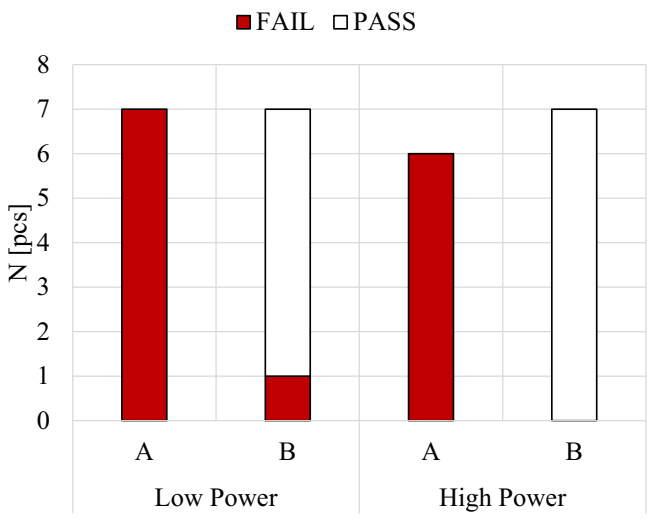

Fig. 5. A summary of the H3TRB test results after 1200 h based on in situ leakage monitoring with $I_r > 2 \times I_{r,\,ref}$ as a failure criterion for booster modules used in 50 kW (low) and 60 kW (high) power converters.

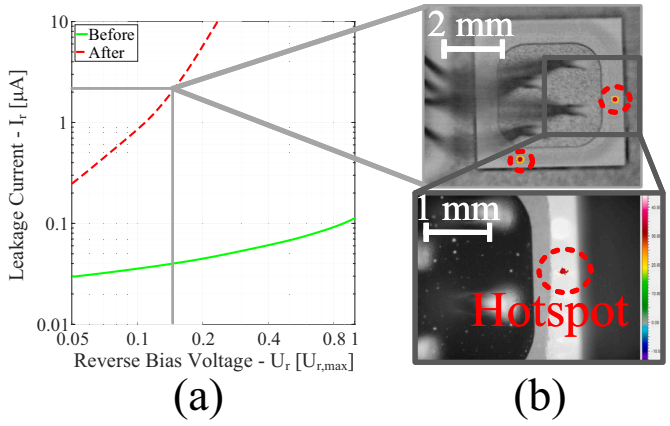

Fig. 6. Device characterisation with (a) a curve tracer showing increased leakage currents and (b) LiT localising the thermal hotspots (the red dashed circles) when biased with $U_r \approx 200$ V (the gray solid line). (For interpretation of the references to colour in this figure legend, the reader is referred to the web version of this article.)

Majority of the failures had short circuit when characterised with the curve tracer. However, four failed samples were only showing major deterioration in leakage characteristics. These failed samples showed visually detectable treelike structures on diode edge termination structures when inspected with optical microscope. It was assumed that these four samples were in earlier stage of the same failure mechanism as most of the failures. Therefore, these four modules were determined to be less damaged and suitable candidates for further failure analysis. After this LiT was used to localise the failure into a single chip, as shown in Fig. 6b. LiT analysis revealed no thermal hotspots in any of the transistor chips (i.e. IGBT or MOSFET) in parallel with the diodes during the test; however, the results consistently showed thermal hotspots on top of the diode chips, both in low- and high-power variants from vendor *A. superior* robustness of IGBT and MOSFET chips could be explained by their different edge termination topologies associated with polyimide passivation. An SEM was used to analyse the hotspot location identified by the LiT analysis in Fig. 6. The SEM analysis (see Fig. 7) revealed that the edge termination region was filled with multiple treelike or dendritic structures, generally spanning out in the direction of the electric field gradient.

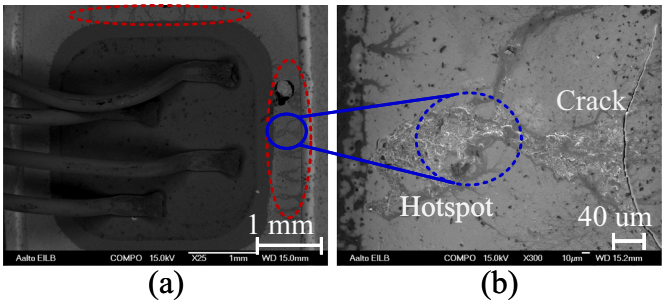

Fig. 7. A top view SEM image shows treelike structures growing (a) all over (the red dotted circles) the top of the glass-passivated diode edge termination while (b) the localised hotspot (the blue dotted circle) shows possible remnants of a highly deformed treelike structure with a visible crack in the glass. (For interpretation of the references to colour in this figure legend, the reader is referred to the web version of this article.)

In regions where treelike structures had grown long enough to cause a local short circuit there were local changes (i.e. cracks in glass passivation and changes in the glass surface morphology). These changes were not observed on shorter treelike structures, which indicate that the changes in morphology and cracks were collateral damage possibly caused by local thermomechanical stresses due to the excess leakage current densities. It became evident that some of the treelike structures seemed to expand over the entire passivation, to the edge of the chip. Generally, the longer structures showed obvious surface deformation of the glass passivation, probably due to the excess leakage power flowing through the structures. However, some of the dendritic structures were much shorter and did not contain any obvious deformation. Further investigation of one of the shorter dendrites after a cross-section (an X-section) was made with a focused ion beam (FIB) revealed that the analysed structure was growing inside the glass passivation, as can be seen in Fig. 8a.

A STEM also confirmed that the dark field (DF) image shows that the dendrite bears no crystalline structure (see Fig. 8b–c), thus, the structure is amorphous, similar to the rest of the glass passivation. The lack of (single or poly-) crystallinity in the treelike structure is contradictory to the failure mechanisms described in the related literature (i.e. ECM of metallic species) [30]. Furthermore, in a recent article the dendrites were described as growing on top of the passivation film rather than inside the solid [7]. The glass passivation showed no signs of porosity and the amorphous treelike structures seemed to be part of the same bulk material.

The material composition was determined using EDX spectroscopy analysis from different orientations on the treelike formation and non-deformed regions of the glass. The EDX analysis from both the top-view results (denoted as T) and the FIB cross-section results (the X-section, denoted as X) suggest that the glass composition changes inside the treelike structure (see Table 2). Based on the SEM + EDX (the T- and

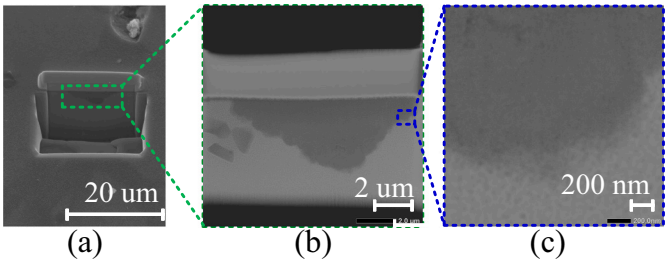

Fig. 8. A FIB X-section shows (a) the treelike structure growing inside the glass rather than on top of it in an SEM image, (b) a lamella made from the X-section shows no inter-boundary phases and (c) the structure is confirmed to be amorphous in a dark field STEM image of the lamella.

Table 2
The EDX spectroscopy average point analysis results show Pb depletion and a Pb/O ratio decrease in the primary trees. (T = Top-view SEM, X = X-Section SEM, L = STEM lamella).

Location	View	Method	at.%		
			O	Si	Pb
Tree	T	SEM + EDX	NA	89	11
Glass	T			82	18
Tree	X			89	11
Glass	X			76	24
Tree	L	STEM+EDX	54	43	3
Glass	L	STEM+EDX	27	36	37

X-views) results, a depletion of Pb was detected inside the formation when compared to the rest of the glass. Furthermore, the STEM+EDX results suggest that the Pb/O ratio decreases inside the dendrite. However, the analysis results do not suggest how the mass balance is fulfilled. To fulfil the mass balance, the most probable explanation would be that the lead has dissolved (i.e. leached) into an electrolytic cell formed by the moisture on top of the glass passivation.

Based on the analysis, the glass passivation most likely consists of a combination of PbO and SiO_2, which are commonly used in lead-silica glass matrices [22]. An elemental mapping of the lamella sample was made with STEM+EDX (see Fig. 9), which highlights the Pb depletion inside the treelike structure.

A closer look at the top-view SEM analysis results show that treelike structures were growing in two directions. The primary (thick) treelike structures were growing in the direction of the anode (towards the edge); the secondary (thinner but denser) treelike structures were barely visible in SEM images and were growing in the reverse direction, as seen in Fig. 10a.

Due to the observed bi-directional growth, ECM is an unlikely explanation for the failure since ECM would require both positively and negatively charged ionic species that are stabile enough to migrate through the pH gradient, as discussed in [7]. This also supports the findings from the STEM analysis that the treelike structures were amorphous, which is contradictory to the literature reporting at least polycrystalline periodicity [30]. The bi-directional growth of treelike

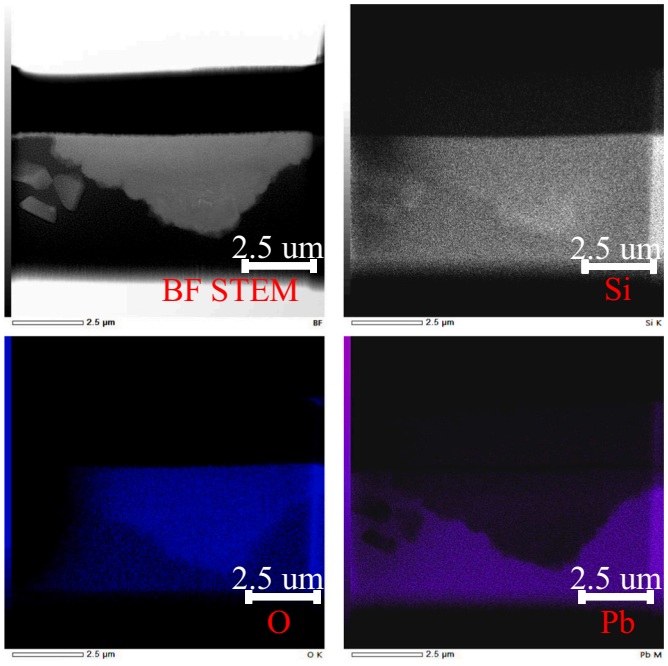

Fig. 9. An elemental mapping of the lamella X-section shows lead (Pb) depletion inside treelike structure using BF STEM EDX spectroscopy analysis.

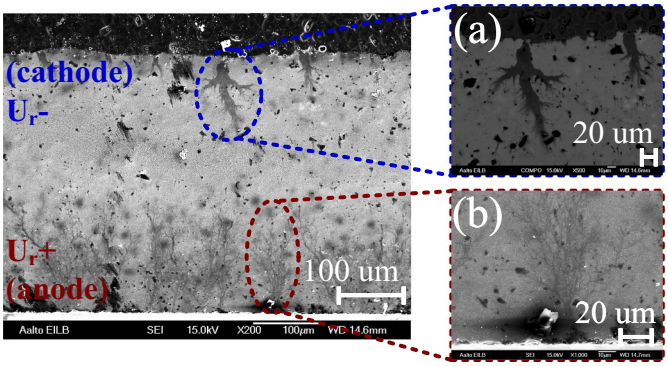

Fig. 10. An SEM image showing both (a) primary cathode (forward) and (b) secondary anode (reverse) treelike structures growing inside the glass passivation.

structures in polyethylene insulators (used in the high voltage power transmission industry) has been reported to be caused by partial discharge (PD) and is described as *electrical treeing* [35]. Furthermore, an IGBT edge termination passivation region is also reported to be prone to failures related to PD [36] and associated bi-directional electrical treeing, which cannot, on the other hand, explain the depletion of lead inside the short treelike structures since it is not known to be associated with electrochemistry [37]. Nevertheless, a similar phenomenon could be a precursor to the PD (i.e. water treeing) [38], a phenomenon which is reported to be similar to electrical treeing on amorphous insulators [37]. The key difference between electrical and water treeing is that the latter requires the presence of moisture and can be associated to electrochemical processes [39]. Water trees can be phenomenologically described as (1) permanent, (2) when humidity and electric field are present, (3) having deteriorated dielectric strength and (4) having increased hydrophilicity [37]. Both electrical and water treeing are also known to deteriorate the insulation properties of the insulator material [35–37]. Furthermore, water treeing may increase the risk for electrical treeing in power semiconductor devices (e.g. power diodes and IGBTs) [40]. Water treeing acts as an aqueous basis for localised electrolytic cell formation [37] and could cause a local dissolution of lead oxide [41,42], leading to lead oxide dissolving (i.e. leaching) into the aqueous solution. This could explain the lack of mass balance in the EDX results in Table 2 and Fig. 9. The leaching of additives (e.g. Boron and Phosphorus) in borosilicate glasses is a known phenomenon [43]. It is also known that lead is highly soluble in water, which is part of the reason why the usage of lead was prohibited in most of electronics manufacturing applications [41,42,44].

Lead monoxide (PbO) is known to be amphoteric, but its Pourbaix (Eh-pH) diagram in moderate concentration H_2O-PbO system is not described in any of the common databases [45,46]. Instead, lead dioxide (PbO_2) is often described [41,45]; however, in [46] lead monoxide was already considered in mild conditions and found to be soluble in alkalic solution. Based on thermodynamic calculations of a moderate PbO (10^{-3} mol/l) concentration in [42], an Eh-pH diagram of an H_2O-PbO system is recreated in Fig. 11a, which is used to emphasise that, in principle, PbO can be immune in range from moderately to highly alkalic solution [42].

However, contradictory to [42], it is suggested in [47] that the stabile region of PbO (s) is shifted closer to the neutral pH and it could also dissolve directly in Pb^{2+}(aq) [46,47]. Nevertheless, the two-phase dissolving process of lead oxide may be responsible for the lower thickness of the secondary (reverse) treelike structures witnessed in Fig. 10b on the anode side. However, there could also be other anodic processes involved in lead glass leaching. Therefore, on the anodic side, a two-phase process maybe involved (see Fig. 11a–b) with the growth of reverse trees, starting with the dissolving of lead oxide into lead hydroxides near neutral pH via the process described in Eqs. (4a) and (4b)

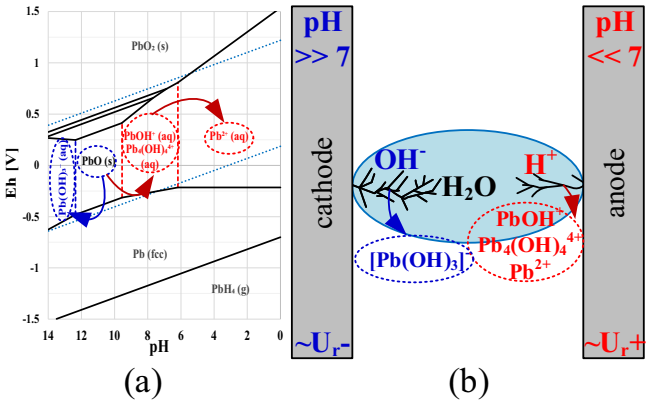

Fig. 11. The EC of lead oxide as described in (a) Pourbaix diagrams of lead oxide (PbO) in a moderate (10^{-3} mol/l) electrolytic aqueous solution at room temperature [42], which acts as a basis for (b) bi-directional water treeing, which can cause localised leaching (e.g. of lead electrochemical corrosion products) [31,42,45].

and finally dissolving via the anodic reactions described in Eqs. (5a) and (5b) into lead ions [42]:

$$PbO(s) + H^+(aq) \leftrightarrow PbOH^+(aq) \quad (4a)$$

$$4PbO(s) + 4H^+(aq) \leftrightarrow {Pb_4(OH)_4}^{4+}(aq) \quad (4b)$$

$$PbOH^+(aq) + H^+(aq) \leftrightarrow Pb^{2+}(aq) + H_2O(l) \quad (5a)$$

$${Pb_4(OH)_4}^{4+}(aq) + 4H^+(aq) \leftrightarrow 4Pb^{2+}(aq) + 4H_2O(l) \quad (5b)$$

Furthermore, it must be noted that the presence of silica in the glass may alter the electrochemistry; however, the effects are believed to be minor due to the stability of silica [46]. The reduction of lead oxide into an alkali solution near the cathode is described clearly in [42], which is most probably responsible for the lead depletion found in forward-growing trees from the cathode:

$$PbO(s) + 2H_2O(l) \leftrightarrow \left[Pb(OH)_3\right]^-(aq) + H^+(aq) \quad (6)$$

Nevertheless, the leaching of lead from the glass phenomenon was studied in the leaching experiments with a moderate concentration (45wt%) of lead-silicate glass, wherein a $t^{1/2}$ law for the lead concentration increase in the solution was observed in the basic (pH = 2) solution [48], which supports the assumption of anodic leaching. Protective measures against leaching for lead glass have also been suggested, either by using a protective film or surface treatment procedures with acetic and hydrochloric acids [49]. These protective methods may be destructive for power semiconductors since an unwanted etching of thin films may occur [50].

4. Conclusion

In this study it was shown that glass passivation can pose a risk to multi-modal failure modes when exposed to the H3TRB-HVDC test conditions. However, only a single failure mechanism was studied in detail from the results of the H3TRB-HVDC test. A voltage blocking degradation, leading finally into a short circuit, was observed in all the tested samples from vendor A with lead glass passivation while PI-based passivation from another vendor seemed to perform better. A LiT analysis suggested that the hotspots were consistently localised onto the high voltage edge termination structures. An SEM analysis confirmed that the edge termination contained several treelike structures growing from both ends of the edge termination on top of the passivation film. However, a further analysis of a cross-section with an SEM revealed that instead of growing on top of the glass passivation, the dendritic structures were growing inside the glass, in contact with the surface, and high-resolution STEM analysis revealed that the dendritic structures were amorphous, thus the failure mechanism could not be associated with ECM or metallic dendrites. EDX analyses revealed the depletion of lead inside the forward-direction dendrites. The most likely explanation for the phenomenon is a localised electrochemical leaching of lead from the glass that is associated with the water treeing phenomenon. Therefore, glass-passivated power semiconductor devices are suggested to be protected if high humidity and high voltage conditions are expected in their application. A further investigation is suggested to compare the performance of the legacy lead glass passivation against modern PI or borosilicate glass passivation techniques. Finally, it is noted that even though the cathodic reaction described in Eq. (6) (i.e. lead glass leaching induced by water treeing) might be the primary mechanism involved with the (forward) treeing, the secondary (reverse) treeing may be caused by another mechanism (e.g. PD or ECM).

CRediT authorship contribution statement

Joonas Leppänen: Conceptualization, Formal Analysis, Investigation, Writing – Original Draft & Review

Glenn Ross: Investigation, Formal Analysis

Vesa Vuorinen: Investigation, Methodology, Supervision, Writing – Review

Jonny Ingman: Investigation, Methodology, Resources, Writing – Review

Joni Jormanainen: Methodology, Resources, Software, Writing – Review

Mervi Paulasto-Kröckel: Supervision, Writing – Review

Declaration of competing interest

The authors declare that they have no known competing financial interests or personal relationships that could have appeared to influence the work reported in this paper.

Acknowledgments

This work has been carried out at ABB Drives and Aalto-University in Finland. The work has been partially funded by the Power2Power project, which is a European co-funded innovation project of the semiconductor industry. The project receives grants from the EU Framework Programme for Research and Innovation H2020, ECSEL Joint Undertaking, and national funding authorities from eight involved countries under grant agreement No. 826417. The participating countries are Austria, Finland, Germany (including the Free States of Saxony and Thuringia), Hungary, the Netherlands, Slovakia, Spain and Switzerland.

References

[1] K. Ma, U.-M. Choi, F. Blaabjerg, Prediction and validation of wear-out reliability metrics for power semiconductor devices with mission profiles in motor drive application, IEEE Trans. Power Electron. 33 (11) (2018) 9843–9853, https://doi.org/10.1109/TPEL.2018.2798585.

[2] D. Zhou, H. Wang, F. Blaabjerg, Mission profile based system-level reliability analysis of DC/DC converters for a backup power application, IEEE Trans. Power Electron. 33 (9) (2018) 8030–8039, https://doi.org/10.1109/TPEL.2017.2769161.

[3] H. Wang, M. Liserre, F. Blaabjerg, Toward reliable power electronics: challenges, design tools, and opportunities, IEEE Ind. Electron. Mag. 7 (2) (2013) 17–26, https://doi.org/10.1109/MIE.2013.2252958.

[4] H. Wang, M. Liserre, F. Blaabjerg, P. de Place Rimmen, Transitioning to physics-of-failure as a reliability driver in power electronics, IEEE J. Emerging Sel. Top. Power Electron. 2 (1) (2014) 97–114, https://doi.org/10.1109/JESTPE.2013.2290282.

[5] A. Hanif, Y. Yu, D. Devoto, F. Khan, A comprehensive review toward the state-of-the-art in failure and lifetime predictions of power electronic devices, IEEE Trans. Power Electron. 34 (5) (2019) 4729–4746, https://doi.org/10.1109/TPEL.2018.2860587.

[6] J. Ingman, J. Jormanainen, A. Vulli, J. Ingman, K. Maula, T. Kärkkäinen, P. Silventoinen, Localization of dielectric breakdown defects in multilayer ceramic capacitors using 3D X-ray imaging, J. Eur. Ceram. Soc. 39 (4) (2019) 1178–1185, https://doi.org/10.1016/j.jeurceramsoc.2018.10.030.

[7] N. Kaminski, C. Zorn, Temperature–humidity–bias testing on insulated-gate bipolartransistor modules – failure modes and acceleration due to high voltage, IET

Power Electron. 8 (12) (2015) 2329–2335, https://doi.org/10.1049/iet-pel.2015.0031.
[8] T. Wassermann, O. Schilling, K. Müller, A. Rossin, J. Uhlig, A new high-voltage H2S single noxious gas reliability test for power modules, Microelectron. Reliab. 100–101 (2019) 113468, https://doi.org/10.1016/j.microrel.2019.113468.
[9] C. Zorn, Alterung von Leistungshalbleitermodulen im Temperatur-Feuchte-Spannungs-Test, Ph.D. thesis, University of Bremen (2019).
[10] J. Jormanainen, E. Mengotti, T. Batista Soreiro, E. Bianda, D. Baumann, E. Friedli, A. Heinemann, A. Vulli, J. Ingman, High humidity high temperature and high voltage reverse bias – a relevant test for industrial applications implemented H3TRB-HVDC tester, in: PCIM Europe 2018, 2018.
[11] C. Papadopoulos, C. Corvasce, A. Kopta, D. Schneider, G. Påques, M. Rahimo, The influence of humidity on the high voltage blocking reliability of power IGBT modules and means of protection, Microelectron. Reliab. 88–90 (2018) 470–475, https://doi.org/10.1016/j.microrel.2018.07.130.
[12] JEDEC, JESD22-A101D – Steady-state Temperature-humidity Bias Life Test, JESD22-A101D, 2015.
[13] IEC, IEC 60749-5:2017: Semiconductor Devices – Mechanical and Climatic Test Methods – Part 5: Steady-state Temperature Humidity Bias Life Test, International Electrotechnical Commission (2017).
[14] C. Papadopoulos, B. Boksteen, G. Påques, C. Corvasce, Humidity robustness of IGBT guard ring termination, PCIM Europe Conference Proceedings (2019) 522–529.
[15] C. Zorn, N. Kaminski, Temperature humidity bias (THB) testing on IGBT modules at high Bias levels, in: International Conference on Integrated Power Systems (CIPS), VDE, 2014.
[16] C. Zorn, N. Kaminski, Acceleration of temperature humidity bias (THB) testing on IGBT modules by high bias levels, Proceedings of the International Symposium on Power Semiconductor Devices and ICs 2015 (2015 June) 385–388, https://doi.org/10.1109/ISPSD.2015.7123470.
[17] J. Leppänen, Humidity Related Failure Mechanisms in Power Semiconductor Devices, Ph.D. thesis, Aalto University (2017).
[18] C. Hu, Modern Semiconductor Devices for Integrated Circuits, Pearson Education, New Jersey, USA, 2010.
[19] J. Lutz, H. Schlangenotto, U. Scheuermann, R. De Donker, Semiconductor power devices-Physics, Characteristics, Reliability, Springer (2011).
[20] N. Mohan, Others, Power Electronics: Converters, Applications and Design, Wiley, 2003.
[21] A. Khosroshahi, M. Abapour, M. Sabahi, Reliability evaluation of conventional and interleaved DC–DC boost converters, IEEE Trans. Power Electron. 30 (10) (2015) 5821–5828, https://doi.org/10.1109/TPEL.2014.2380829.
[22] SCHOTT, SCHOTT Technical Glasses – Physical and Technical Properties, Tech. rep, SCHOTT North America Regional Research & Development, 2014.
[23] D. Askeland, P. Pradeep, J. Wendelin, The science and engineering of materials, 6th Edition, Global Engineering, 2010.
[24] R. W. Revie, Uhlig's Corrosion Handbook, 3rd Edition, John Wiley & Sons, Inc., Hoboken, NJ, USA, 2011. ar Xiv:arXiv:1011.1669v3 , doi:https://doi.org/10.1002/9780470872864.
[25] W. Schmickler, E. Santos, Interfacial Electrochemistry, Springer, 2010.
[26] V. Boisson, M. Le Helley, J.-P. Chante, Computer study of a high-voltage a p-π-n–n+diode and comparison with a field-limiting ring structure, IEEE Trans. Electron Devices 33 (1) (1986) 80–84.
[27] M.R. Awode, Introduction to Electrochemistry, Himalaya Pub, House, 2010.
[28] D. Minzari, M.S. Jellesen, P. Møller, R. Ambat, On the electrochemical migration mechanism of tin in electronics, Corros. Sci. 53 (10) (2011) 3366–3379, https://doi.org/10.1016/j.corsci.2011.06.015.
[29] X. Zhong, L. Chen, B. Medgyes, Z. Zhang, S. Gao, L. Jakab, Electrochemical migration of Sn and Sn solder alloys: a review, RSC Adv. 7 (45) (2017) 28186–28206, https://doi.org/10.1039/c7ra04368f.
[30] M. Sun, H.-G. Liao, K. Niu, H. Zheng, Structural and morphological evolution of lead dendrites during electrochemical migration, Sci. Rep. 3 (1) (2013) 3227, https://doi.org/10.1038/srep03227.
[31] V.S. Bagotsky, Fundamentals of Electrochemistry, Wiley-Interscience, 2005.
[32] R. Newman, Pitting corrosion of metals, Electrochem. Soc. Interface 19 (1) (2010) 33–38, https://doi.org/10.1149/2.F03101IF.
[33] W.D. Callister, Fundamentals of Materials Science and Engineering, 5th Edition, Wiley, 2016.
[34] H. Preu, W. Mack, T. Kilger, B. Seidl, J. Walter, P. Alpern, M. Kirchberger, Root cause finding of a diode leakage failure using scanning magnetic microscopy and ToF-SIMS as key methods, in: Conference Proceedings From the International Symposium for Testing and Failure Analysis, 2006.
[35] H. Zheng, S.M. Rowland, I. Iddrissu, Z. Lv, Electrical treeing and reverse tree growth in an epoxy resin, IEEE Trans. Dielectr. Electr. Insul. 24 (6) (2017) 3966–3973, https://doi.org/10.1109/TDEI.2017.006729.
[36] P. Fu, Z. Zhao, X. Cui, T. Wen, H. Wang, X. Li, P. Zhang, Partial discharge measurement and analysis in high voltage IGBT modules under DC voltage, CSEE Journal of Power and Energy Systems 4 (4) (2018) 513–523. doi:10.17775/cseejpes.2017.01190.
[37] R. Ross, Inception and propagation mechanisms of water treeing, IEEE Trans. Dielectr. Electr. Insul. 5 (5) (1998) 660–680, https://doi.org/10.1109/94.729689.
[38] T. Miyashita, T. Inoue, Treeing phenomena in polyethylene-coated wire immersed in water, Electr. Eng. Jpn. 90 (3) (1970) 83–91.
[39] J.G. Drobny, Polymers for Electricity and Electronics: Materials, Properties, and Applications, John Wiley and Sons, Hoboken, NJ, USA, 2012, https://doi.org/10.1002/9781118160121.
[40] J.H. Fabian, S. Hartmann, A. Hamidi, Analysis of insulation failure modes in high power IGBT modules, in: Conference Record - IAS Annual Meeting (IEEE Industry Applications Society), 2005, https://doi.org/10.1109/IAS.2005.1518425.
[41] Y. Xie, Dissolution, Formation, and Transformation of the Lead Corrosion Product PbO2: Rates and Mechanisms of Reactions That Control Lead Release in Drinking Water Distribution Systems, doctoral thesis, Washington University (2010).
[42] P.A. Nikolaychuk, The revised potential – pH diagram for Pb – H2O system, Ovidius University Annals of Chemistry 29 (2) (2018) 55–67, https://doi.org/10.2478/auoc-2018-0008.
[43] V.Y. Vasilyev, Borophosphosilicate Glass Thin Films in Electronics, Nova Science Publishers, 2013.
[44] O. Deubzer, Y. Baron, N. Nissen, K.D. Lang, Status of the RoHS directive and exemptions, in: 2016 Electronics Goes Green 2016+, EGG 2016, IEEE, 2017, https://doi.org/10.1109/EGG.2016.7829868.
[45] N. Takeno, Atlas of Eh-pH diagrams Intercomparison of thermodynamic databases, National Institute of Advanced Industrial Science and Technology Tokyo (419) (2005) 285.
[46] M. Pourbaix, Atlas of Electrochemical Equilibria in Aqueous Solutions, National Association of Corrosion Engineers, Houston, Texas, USA, 1974.
[47] W. Zhang, S. Haskouri, G. Houlachi, E. Ghali, Lead-silver anode behavior for zinc electrowinning in sulfuric acid solution, Corros. Rev. 37 (2) (2019) 157–178, https://doi.org/10.1515/corrrev-2018-0007.
[48] R. Bertoncello, L. Milanese, A. Bouquillon, J.C. Dran, B. Mille, J. Salomon, Leaching of lead silicate glasses in acid environment: compositional and structural changes, Appl. Phys. Mater. Sci. Process. 79 (2) (2004) 193–198, https://doi.org/10.1007/s00339-004-2651-9.
[49] L. Rybaříková, L. Dvorská, H. Hradecká, P. Jiříček, Surface treatment of lead glasses for reducing the leaching of lead, Ceramics-Silikáty 45 (1) (2001) 31–34.
[50] S. Franssila, Introduction to Microfabrication, John Wiley & Sons, Ltd, Helsinki, Finland, 2010.